PROCEEDINGS, 41st Workshop on Geothermal Reservoir Engineering
Stanford University, Stanford, California, February 22-24, 2016
SGP-TR-209

Simple Analytics for EGS:

Quantifying Wellbore-centric Crustal Heat Extraction by Peclet Parameters

Peter Leary and Peter Malin

Helmholtz Centre Potsdam GFZ German Research Centre for Geosciences, Telegrafenberg, 14473 Potsdam, Germany

p.leary@auckland.ac.nz pem@asirseismic.com

Keywords: EGS, Peclet number, heat transport, wellbore flow, wellbore stimulation, permeability stimulation

ABSTRACT

As with all EGS schemes, wellbore-centric heat extraction is subject to heat supply by conduction rather than by advected heat transport as with naturally convective geothermal systems. The impact of a conductive rather than a convective heat flow boundary is, however, not widely recognised. This omission can be remedied by analytic solutions for simple 2D steady-state and time-evolving wellbore-centric radial flow heat transport parameterized by a dimensionless Peclet number, $\gamma \equiv v_0 r_0/D$. Peclet number $\gamma \equiv v_0 r_0/D$ is the ratio of radial flow heat advection -- given by the product $v_0 \cdot r_0$ [m^2/s] of radial heat advective Darcy fluid velocity v_0 at characteristic flow system radius r_0 -- and intrinsic thermal diffusivity of the rock-fluid system, $D \equiv K/\rho_w C_w$ [m^2/s]. For a flow medium of porosity φ, Darcy fluid flow velocity is given in terms of bulk seepage flow v_s, $v_0 \equiv v_s/\varphi$. The effective crustal diffusivity $D \sim 0.7 \cdot 10^{-6} m^2/s$ is given by the thermal conductivity of rock $K \sim 3 W/m \cdot {}^oC$ and the volumetric heat capacity $\rho_w C_w \sim 4\ 10^6 J/m^3 \cdot {}^oC$ of the heat-transporting pore water.

Radial flow Peclet parameter γ relates directly to wellbore-centric heat production. A normative ℓ = 1km-long horizontal wellbore in a uniform crustal volume of porosity φ and advective fluid heat capacity $\rho_w C_w$ at temperature $T_0 = 100^oC$ produces heat energy at rate $Q = 2\pi\varphi r_0\ v_0\ \ell\ \rho_w C_w\ T_0$ [W]. For $Q \sim 1MW$ in a wellbore of radius r_0 and Darcy velocity v_0, Peclet number $\gamma = v_0 r_0/D = r_0 v_0\ (\rho_w C_w/K) = Q/(2\pi\varphi \ell K T_0) \sim 10/6\pi\varphi$ has magnitude $\gamma \sim 5$ for crustal porosity $\varphi \sim 10\%$. The volume rate of fluid flow producing $Q \sim 1MW$ heat energy flow is $V = 2\pi\varphi r_0 v_0 \ell = 2\pi\varphi\gamma D\ell \sim 2L/s$. Increased advective fluid flow velocity v_0 from the crustal volume into the wellbore producing $Q \sim 10MW$ of heat energy has Peclet number $\gamma \sim 50$ and wellbore volume flow rate 20L/s.

To investigate the implications of Peclet number ~ 5, we begin with steady-state radial flow heat transport solutions in 2D proceeding from conservation of heat energy for wellbore-centric radial flow. In analogy with the Bredehoeft & Papadopulos (1965) 1D temperature distribution for steady-state planar groundwater flow with Peclet number $v_0\ell/D$ in terms of Darcy fluid velocity v_0 in a crustal layer of thickness ℓ with water-rock system thermal diffusivity $D \equiv K/\rho C$, solutions for 2D cylindrical and 3D spherical radial flow in a uniform medium have Peclet number $\gamma = v_0 r_0/D$ for respective radial fluid velocity fields $v(r) \equiv v_0 r_0/r$ and $v(r) \equiv v_0 r_0^2/r^2$ centered on an inner radius r_0 flow boundary at temperature T_0 and outer radius r_1 flow boundary at temperature T_1. The steady-state temperature field for a 2D cylindrically-symmetric heat advection flow system with Peclet number γ applicable to advective heat transport to horizontal long-reach wellbore intervals is

$$T(r) = T_0 + (T_1 - T_0) \cdot ((r/r_0)^\gamma - 1)/((r_1/r_0)^\gamma - 1).$$

For conduction-dominated Peclet numbers with low advection fluid flow rates $\gamma < 1$, steady-state heat extraction in a crustal volume subject to conductive recharge has high rates of change of spatial temperature gradient near the wellbore. As advective fluid flow velocity increases to higher advection fluid flow rates $\gamma > 1$, the system temperature gradient moves outward from the vicinity of the wellbore to the vicinity of the bounding outer radius r_1. We are interested in the scale of the outer radius r_1 implied by a given Peclet number.

The spatiotemporal scale at which heat advection cools crustal rock from the vicinity of a wellbore outward is obtained from the time-evolving equation of heat conservation in an infinite medium with interior temperature/flow boundary at the wellbore set by Peclet number γ. For an instantaneous line-source heat pulse at the wellbore, the temperature field evolves temporally and spatially as $exp(-r^2/4Dt)/4Dt$. Significant wellbore-centric heat advective flow associated with Peclet number γ modifies conduction thermal evolution by weighting function $(r^2/4Dt)^{\gamma/2}$. For conduction dominated systems, $\gamma < 1$, at times $t > 0$ immediately following an instantaneous line-source heat pulse, temperatures near the wellbore decay slowly $T(r,t) \propto exp(-r_0^2/4Dt)/4Dt \sim (1 - r_0^2/4Dt)/4Dt$. As with steady-state solutions, radial heat advection, $\gamma > 1$, causes crustal volume temperature distributions in which the r_0 boundary temperature T_0 moves increasingly towards the outer boundary radius r_1.

Solution form $exp(-r^2/4Dt) \cdot (r^2/4Dt)^{1+\gamma/2}$ applied to an unbounded radial flow system centered on a constant wellbore boundary temperature T_0 characterizes the spatiotemporal scale of wellbore-centric EGS heat extraction volumes. Durable heat supply from a conductively charged EGS crustal volume requires that (i) a given Peclet parameter support advective heat flow at a sufficient radius from the central heat extraction wellbore; and (ii) low-porosity/low-permeability crust be stimulated to the radial extent required by the

Peclet number flow. Flow for Peclet parameter $\gamma \sim 5$ in a crustal volume of porosity $\varphi \sim 10\%$ requires a wellbore-centric crustal heat exchange volume to be stimulated to a radius 25-50 meters. The technical challenge for EGS crustal heat volume stimulation is gauged by observing fluid production from low-porosity ($\varphi \sim$ 5-8%)/low-permeability (pre-stimulation $\kappa \sim$ 100nanoDarcy) clastic-based shale formations. Modelling oil/gas/water decline curves from shale formations subjected to standard wellbore-centric hydrofracture stimulation indicates that effective rock-flow stimulation extends radially to perhaps a 20m and axially to perhaps 5m. The indicative stimulation volume of wellbore-centric crustal rock permeability achieved by existing hydrofracture practice applied at 50m wellbore intervals in clastic-based shales is a small fraction of the stimulation volume needed for commercial EGS heat extraction characterised by relatively low Peclet number $\gamma \sim 5$.

1. INTRODUCTION

Tester et al. (2006) summarize a long-standing concept of how abundant stores of heat energy at 3km-5km depths can be accessed through large scale engineering interventions in crustal rock flow structure. The concept assumes that hydraulic fracturing can generate large, well-connected planar flow surfaces at which moving fluids absorb heat stored in intervening crustal slabs and transport the heat to wellbore conduits that rise to the surface:

> *The heat-transfer system can be thought of as similar to a series of flat plates with gaps (the fractures) between them and a semi-infinite conduction heat source surrounding each fracture. Heat is transferred by conduction through the rock, perpendicular to the surfaces of the fractures.*

A number of experimental heat extraction sites such as Fenton Hill, Rosemanowes, Soultz, Basel and Paralana are based on this concept. As noted by Moeck & Beardsmore (2014) and Bertani (2015), however, heat production at such crustal hydrofracture stimulation sites has been distinctly limited: ~ 40MWe of electrical power generation at some 10 sites compared with ~ 12GWe electricity production at some 175 natural geothermal systems.

Given the evident complexity of fracture stimulation in crustal rock (e.g., Jason 2014; cf. Leary 1997, 2002; Leary et al. 2015; Malin et al. 2015; Pogacnik et al. 2015), it is sensible to revisit crustal heat extraction in terms of a more limited assumption set than that of Tester et al. (2006). We assume here only that narrow-gauge wellbores are a necessary, direct and integral component of deep crustal heat extraction systems, and that the narrow-gauge wellbores can be used to support hydrofracturing operations to stimulate permeability in the surrounding crust. Focusing on wellbore-centric flow in uniform media reduces EGS considerations from 3D to 1D radially-symmetric flow that is (i) subject to elementary temperature and fluid flow mechanics, boundary conditions, and potential observation, and (ii) allows calibration of wellbore-centric permeability stimulation based on existing hydrofracture practice in clastic-like hydrocarbon-bearing shale formations. In this paper we discuss:

- Simple analytic expressions for steady-state heat transport in wellbore-centric radially-symmetric flow systems;
- Analytic expressions for spatiotemporal evolution of a temperature field for a fixed wellbore-centric temperature line-source in an infinite uniform crustal porous medium;
- Oil/gas/water decline curve data from clastic-like shales subject to wellbore-centric hydrofracture stimulation that calibrate the effective radial and axial extent of flow enhancement achieved by existing technology and practice.

Steady-state and time-evolving wellbore-centric radial flow heat transport temperature distributions are characterised by a single dimensionless parameter $\gamma \equiv v_0 r_0/D$ that is directly tied to heat extraction for an EGS wellbore. Time-evolving temperature fields determined by γ calibrate the radial flow dimension needed for a given commercial geothermal wellbore power production fixed by γ. Analysis of oil/gas/water production decline-curve data based on flow into a wellbore from a narrow radial fracture in a stimulated crustal volume indicates that the radial spatial extent of existing frack-stimulation technology may be extremely limited relative to wellbore-centric flow-stimulation crustal heat exchange volumes needed for commercial EGS heat extraction.

2. HEAT ADVECTION FOR CYLINDRICAL AND SPHERICAL RADIAL FLOW IN UNIFORM MEDIA

Advective heat transport by radial fluid flow to/from a wellbore is conveniently introduced by reference to the Bredehoeft and Papadopulos 1965 discussion of heat transport by water moving in a plane-layered crust. Conservation of steady-state heat energy advection in a plane-layered earth between $0 \leq z \leq \ell$

$$\partial_z^2 T = v_0 \rho C/K \, \partial_z T, \tag{1}$$

constrains the layer temperature distribution in terms of constant vertical groundwater velocity v_0, thermal conductivity of rock $K \sim$ 3W/m·^{o}C, and the density and heat capacity of water $\rho \sim$ 1000kg/m^3 and $C \sim$ 4280J/kg·^{o}C. The resulting temperature field can be written

$$T(z) = T_0 + (T_L - T_0)(e^{\beta z/\ell} - 1)/(e^{\beta} - 1), \tag{2}$$

where the dimensionless ratio of heat transport $v_0\rho C$ to heat conduction K/ℓ appears as $\beta \equiv v_0\rho C\ell/K$. The ratio β in advective heat transport is commonly denominated as the Peclet number characterizing the advection system. As β is proportional to advective flow velocity v_0, low Peclet numbers denote conduction-dominated flow, and high Peclet numbers denote advection-dominated systems. As a consequence of steady-state flow, the fluid velocity and heat transport across the layer are constant, and equal to $v(z) \equiv v_0$ from the conservation of mass condition $\nabla \cdot \boldsymbol{v}(\boldsymbol{x}) = \partial_x v_x + \partial_y v_y + \partial_z v_z = 0$.

Consider now a steady-state radially symmetric temperature field $T(r)$ centered on a wellbore of radius r_0. From the surrounding crust, fluid flow extracts heat at a steady-state rate $q(r_0)$ [W/m^2] due to radially symmetric fluid flow $v(r) = v_0 r_0/r$ into the wellbore. The components of radial heat transport are thermal conduction $K\partial_r T(r)$ and thermal advection $\rho C v(r) T(r)$,

$$q(r) = K\partial_r T(r) - \rho C v(r) T(r), \tag{3}$$

for rock thermal conductivity $K \sim 3$W/m/^{o}C and the volume heat capacity of water $\rho C \sim 4$ MJ/m^3·^{o}C.

In absence of crustal heat energy sources, conservation of heat energy $\nabla \cdot \boldsymbol{q}_A(r) = 0$ leads to radial temperature distribution condition

$$\nabla^2 T(r) = \partial_r{}^2 T(r) + 1/r\, \partial_r T(r) = \rho C/K \cdot v_0 r_0/r \cdot \partial_r T(r),$$

defining the following condition on radially symmetric temperature gradients,

$$\partial_r{}^2 T(r) = (v_0 r_0 \rho C/K - 1)/r \cdot \partial_r T(r). \tag{4}$$

In (4), the rate of change of radial temperature gradient is proportional to the radial temperature gradient and inversely proportional to the distance from the wellbore. Large temperature gradients at small flow radii associated with wellbores imply reduced heat content in the vicinity of wellbores. Groundwater and hydrocarbon extraction flow face no such energy-content degradation.

Steady-state radial heat advection across a cylindrical section about a central well axis driven by temperatures $T(r_0) = T_0$ and $T(r_1) = T_1$ at inner and outer radii respectively given by (4) is

$$T(r) = T_0 + (T_1 - T_0)\cdot((r/r_0)^\gamma - 1)/((r_1/r_0)^\gamma - 1), \tag{5}$$

where the dimensionless parameter $\gamma \equiv v_0 r_0/D$ defines the flow system effective Peclet number. The Peclet number denotes the ratio of advective fluid flux $v_0 r_0$ at radius r_0 to effective thermal diffusivity of the water-rock system $D \equiv K/\rho C \sim 0.7\ 10^{-6}$ m^2/s. Large values of γ denote high degrees of advected heat relative to thermally conducted heat, and low values of γ denote heat transport dominated by thermal conduction. Complementing cylindrical steady-state heat advection temperature profile (5) is its spherical analogue $T^S_0 \le T^S(r) \le T^S_1$ for radial shells centered on a central sphere of radius r_0,

$$T^S(r) = T_0 + (T_1 - T_0)\cdot(exp(\gamma(r_0/r - 1)) - 1)/(exp(\gamma(r_0/r_1 - 1)) - 1), \tag{6}$$

where the Peclet number for spherically symmetric radial flow is the same as that for cylindrically symmetric radial flow.

The associated Darcy radial flow velocity fields associated with cylindrical and spherical heat advection temperature fields (5) and (6) are respectively $v(r) = v_0 r_0/r$ and $v(r) = v_0 r_0{}^2/r^2$, with advected heat $q(r) = K\partial_r T(r) - \rho C v(r) T(r)$ having the form of thermal conduction with heat flux magnitude $q(r) = q_0 r_0/r$ and $q(r) = q_0 r_0{}^2/r^2$respectively. Typically in situations of interest, $|q(r)| \sim \gamma/r\ KT_0 = q_0 r_0/r$ with $q_0 = v_0 \rho C T_0$. Appendix 1 gives details for (3)-(6).

Fig 1 illustrates the radial temperature profiles associated with heat transport for 1D radially symmetric advective cylindrical flow. Temperature profiles are shown for a sequence of advective flow velocities appearing in Peclet parameter $\gamma \equiv v_0 r_0/D$. The temperature profiles in blue progress from highly advective velocities, $\gamma > 1$, at right to increasingly conductive advection at left, $\gamma < 1$. Zero advective velocity, $\gamma = 0$, merges with the conductive temperature profile in red the far left. As indicated by (5), the advective velocity corresponding to Peclet parameter $\gamma = 1$ corresponds to a constant thermal gradient denoted in cyan across the radial interval.

The essential feature of advective heat transport, $\gamma > 1$, is that the temperature gradient in the heat transport system is moved away from the wellbore to the periphery of the flow system. The temperature at the wellbore is determined by the rate at which heat is removed from the crustal volume $q_0 = \gamma/r_0\ KT_0 = v_0 \rho C T_0$. To sustain the heat flow exiting at the wellbore at T_0, the outer boundary of the flow system must be maintained at a fixed temperature T_1 by heat arriving from the embedding crustal volume. We next estimate the wellbore-centric crustal volume radius needed to sustain an outer boundary temperature T_1 for a commercially relevant period of time.

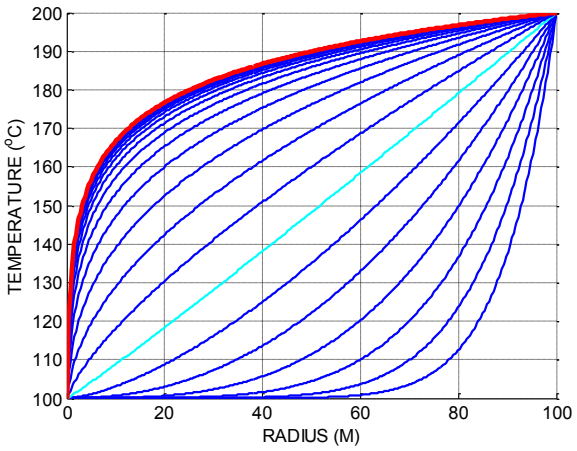

Figure 1: Illustration of steady-state cylindrically-symmetric radial temperature profiles (5) for a range of Peclet parameter γ governing advective flow from outer radius r_1 = 100m at temperature T_1 = 200°C to inner radius r_0 = 0.1m at temperature T_0 = 100°C. The range of profiles in blue is from γ = 10 at right to γ = 0 at left. The profile for γ = 0 overlays the purely conductive heat transfer given in red. As evident from (5) the linear radial temperature profile in cyan is for γ =1. At high advective flow, the thermal gradient is close to the outer system radius. At low advective flow, the thermal gradient is close to the inner system radius.

3. TIME-EVOLVING ADVECTION FOR CYLINDRICAL RADIAL FLOW

Steady-state advective flow in a 1D radial geometry as pictured in Fig 1 can be generalized to allow for time evolution of heat supplied to or extracted from an EGS crustal heat exchange volume. We first consider an initial state of an unbounded wellbore-centric crustal volume of uniform properties into which a heat pulse is injected instantaneously by an axial source of heat production Q per unit length. As given in Appendix 2, without advective flow the 1D spatiotemporal temperature response of the wellbore-centric radially symmetric uniform medium of thermal diffusivity D is $Q/4\pi Dt \cdot exp(-r^2/4Dt)$. While purely thermal conduction processes in rock are defined by diffusivity $D_r \equiv K/(\rho_r C_r) \sim 3 \text{W/m·°C}/2400 \text{kg/m}^3/840 \text{J/kg·°C} \sim 1.510^{-6}$ m^2/s, the presence of significant water flowing in rock modifies the effective thermal properties. For significant advection, radial heat transport associated with a central wellbore is quantified by the lower diffusivity occasioned by the high heat capacity of water, $D \equiv K/(\rho_w C_w) \sim 0.7 \cdot 10^{-6}$ m^2/s. As noted in Appendix 2, the solution of the time-dependent version of the steady-state modified Bessel equation (4) gives the time-evolving temperature field in the presence of advective heat transport in the form of weighting factor $W \equiv (r^2/4Dt)^{\gamma/2}$ applied to the standard time-evolution term $Q/4\pi Dt \cdot exp(-r^2/4Dt)$,

$$T(r,t) \propto 1/t \; exp(-r^2/4Dt) \cdot (r^2/4Dt)^{\gamma/2}. \qquad (7)$$

Fig 2 shows time-evolving radial temperature profiles (7) for radial advection heat transport due to an instantaneous pulse of line-source temperature drop in an infinite uniform medium of thermal diffusivity $D \sim 0.7 \cdot 10^{-6}$ m^2/s. Each trace registers temperature recovery from the effects of the wellbore cooling pulse; blue traces show thermal recovery due to conduction, γ = 0, red traces show recovery due to moderate advection, γ = 3, and black traces due to higher advection, γ = 10. (For simplicity, the cooling event temperature responses at small radii are not shown.) Without advection, the instantaneous wellbore temperature drop is confined to the wellbore vicinity and gradually recovers as heat is conducted towards the wellbore. With advection, the instantaneous wellbore temperature drop propagates into the medium (not shown) and then recovers as heat is advected inwards towards the wellbore. The radial scale of the temperature recovery increases with as the square root to elapsed time from 1 year at the upper left to 25 years at the lower right. The radial scale of heat mobility is essentially proportional to the Peclet number $\gamma \equiv v_0 r_0/D$, reflecting its dependence on the velocity of advective fluid v_0.

The relation of the time-evolving conductive and advective radial temperature profiles in Fig 2 bear a general resemblance to the low advection and high advection steady-stare profiles of Fig 1, reflecting the different spatiotemporal rates at which heat is moved by advection fluids. With EGS heat extraction requiring adequate advective flow through permeability stimulation of a crustal volume, it is important to assess the radial extent of the heat-exchange volume and the rate at which fluid flows through the volume that is implied by any particular Peclet number.

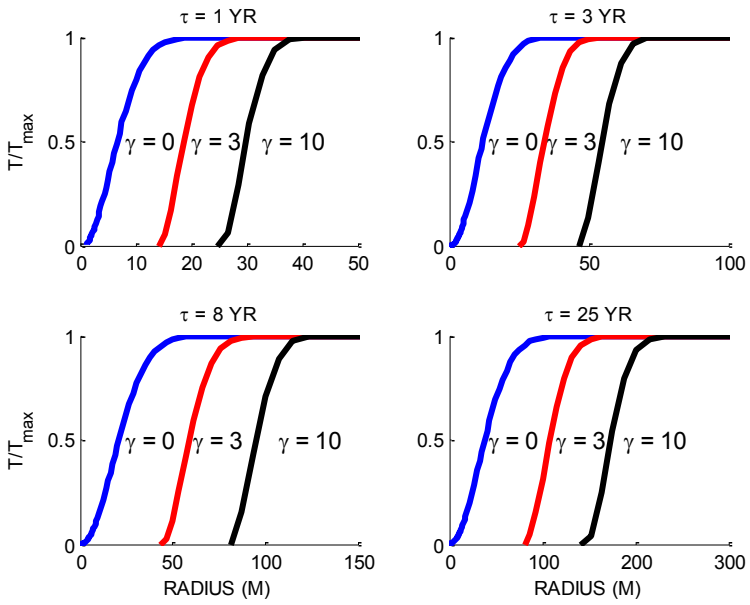

Figure 2: Snapshots of time-evolving temperature profiles (7) for wellbore-centric cylindrically-symmetric flow for three Peclet numbers γ = [0 3 10] registered at four periods of elapsed time since an instantaneous wellbore-centric line-source temperature cooling pulse. At each snapshot time τ = [1 3 8 25] years, blue trace radial profiles for conductive heat flow move slowly outwards from the wellbore, while the red and black radial profiles for advective heat transport move more quickly, essentially in proportion to the Peclet number. For simplicity the small-radius cooling event is not shown. The restoration of heat lost due to the instantaneous cooling pulse is supplied the surrounding crust. EGS stimulation must be compatible with the spatiotemporal scales of heat movement implied by a given Peclet number.

The Fig 2 heat recovery curves for the instantaneous cooling impulse illustrate the spatiotemporal scales by which heat advection accelerates the transfer of crustal heat as a function of Peclet number. We now assess the physical scale of an EGS flow system needed to supply the advective heat by determining the crustal heat transfer response to a permanent wellbore temperature change. The spatiotemporal evolution of a temperature field associated with advecting heat in an infinite medium centered on a wellbore of radius r_0 that is maintained at fixed temperature T_0 is given in Appendix 2,

$$T(r,t) = T_0 + 2/\pi \cdot T_0 \, (r/a)^{\nu} \int dk/k \, exp(-k^2 Dt) \, (J_\nu(kr)Y_\nu(ka) - Y_\nu(kr)J_\nu(ka))/(J_\nu^2(ka) + Y_\nu^2(ka)^2), \qquad (8)$$

where $J_\nu(kr)$ and $Y_\nu(kr)$ are respectively order-ν Bessel functions of the first and second kind, $\nu \equiv \gamma/2$, and k is an inverse wavelength over which the Bessel function weights are summed for selected times t at selected radii $r_0 = 1\text{m} < r < r_1 = 10^4\text{m}$.

In Fig 3 we see temperature spatial distribution snapshots for (8) at times [5, 10, 25, and 50] years for low advection, Peclet number $\gamma \sim 0$, in blue and moderate advection, $\gamma \sim 4$, in red. At each time, the evolving radial temperature distributions in Fig 3 resemble the Fig 1 steady-state temperature distributions. Fig 3 blue traces correspond to $\gamma = 0$ thermal conduction having the shape of the left-hand Fig 1 traces, and Fig 3 red traces corresponding to $\gamma = 4$ have the higher advection shape of the right-hand Fig 1 traces. Unlike Fig 1, however, the Fig 3 spatiotemporal scales reflect different degrees of heat transport as functions of time and space. In particular, Fig 3 illustrates that if an EGS system is to extract crustal heat for a 50 year period, it must have a radial stimulation dimension of order 20m. However, the advective heat evolution model (8) implicitly assumes that heat and fluid are available from beyond the radius at which heat evolution is evaluated. Hence the 20m radius heat-exchange stimulation volume must be embedded in a crustal volume which minimally supplies heat and fluid to the interior heat-exchange volume through conduction and possible advection. For a wellbore-centric heat-extraction system that is essentially stable for wellbore-centric heat extraction periods ~ 30-50 years, the supporting crustal fluid flow system and conductive heat supply must be in well in excess of 20-25 meter radius.

Fig 3 also quantifies the extent to which advective heat extraction produces heat from the crust. In any given period, low advection $\gamma \sim 0$ consistent with thermal conduction produces heat from approximately one quarter to one tenth of the crustal volume that produces heat by advective flow for Peclet number $\gamma \sim 4$.

The Fig 1-3 EGS scenario can be contrasted to the nature of crustal heat supply in the naturally convective hydrogeothermal flow systems that currently produce the vast bulk of geothermal energy presently available. For naturally occurring convective flow, the produced heat is simply tapped off a far more powerful natural advection system.

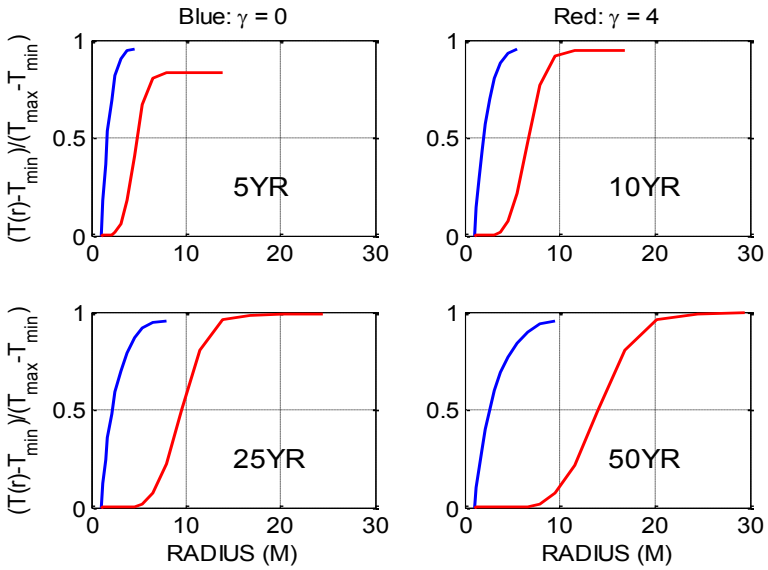

Figure 3: Illustration of time-evolving cylindrically-symmetric radial temperature profiles (8) for Peclet parameter values γ = 0 (blue) and γ = 4 (red) at four periods of spatiotemporal heat flow evolution, τ = [5 10 25 50] years. Each pair of blue and red curves reprises the low-advection and higher-advection limits of the Fig 1 steady-state radial temperature profiles. As seen in the lower right plot, a steady-state approximation to EGS heat extraction with a life-time of order 50 years requires a stable heat-exchange elevated-flow-stimulation volume of order 20m radius. That heat-exchange volume must be embedded in the functional equivalent of an infinite heat reservoir for the period of time that heat is extracted.

4. PROSPECTS FOR EGS PERMEABILITY STIMULATION IN LIGHT OF SHALE FORMATION PRODUCTION FLOW

Figs 1-3 illustrate spatiotemporal scales of elementary wellbore-centric EGS crustal heat extraction for a uniform porous flow medium of effective rock-water system thermal diffusivity $D \sim 0.7{\cdot}10^{-6}$ m^2/s. Wellbore heat production defined by dimensionless Peclet parameter $\gamma \equiv v_0 r_0/D$ in terms of fluid velocity v_0 at wellbore radius r_0 indicates that a radial heat extraction system $\gamma \sim 5$ sufficient to supply 1MW of thermal output for a period of decades requires a wellbore-centric radial dimension of order 20 to 50 meters in order to maintain sufficient boundary crustal heat flux and temperature for a commercially relevant period of time.

EGS projects designed for deep low porosity and permeability rock presuppose engineering intervention to create adequate flow velocity over a sufficient radius to establish a conductive heat supply approximating an infinite reservoir. EGS prospects depend on the means by which permeability enhancement can be achieved. Oil/gas/water production curves from hydro-fractured shale formations provide the basis for estimating the radial extent that current hydrofracture technology creates wellbore-centric permeability enhancement. The hydrofracture stimulation process creates a radially-symmetric flow structure whose post-stimulation drainage history can be modelled in physical terms compatible with the radially-symmetric heat transport framework (3)-(8).

Radial diffusion flow into a central wellbore from a pressurized wellbore-centric fracture-plane normal to the wellbore occurs in three stages. The first stage begins at zero flow rate when the wellbore is first allowed to flow, with flow then increasing as the pressurized fluid in the stimulated fracture begins to diffuse out of the fracture into the wellbore. The second flow stage begins when the first stage flow peaks at a characteristic time τ_0 and begins to decline until the fluid flow in the stimulated fracture equilibrates with the ambient pressure. The third stage begins when fluids leak out of the formation into the fracture with characteristic time τ_∞.

The three-stage stimulated-fracture fluid drainage sequence can be modelled in diffusion terms derived from conservation of mass, (9)-(18) below, in a manner similar to that of conservation of heat energy, (3)-(8) above. Wellbore fluid production histories from nine production wells in clastic-like hydrocarbon-bearing shales return the second and third flow stage time constants τ_0 and τ_∞ and allow estimation of three effective flow system parameters:

- $\tau_0 \sim 20 \pm 10$ days, fixed by the time at which wellbore flow switches from initial-state incline to final-state decline;
- $\tau_\infty \sim 100 \pm 60$ days for oil/gas and $\tau_\infty \sim 370 \pm 250$ days for water, fixed by the times wellbore flow reaches final-state drainage rate;
- Effective frack-formation flow system radius $R_{sys} \sim 20$m for oil/gas flow and R ~ 10m for water flow;
- Effective frack-formation diffusivity $D_{sys} \sim 1\text{-}2{\cdot}10^{-4}$m^2/s for all fluids;
- Enhanced effective permeability $\kappa_{sys} \sim 1\text{-}2{\cdot}10^{-17}$m^2 (10-20μDarcy) for all fluids

By Darcy's law, crustal fluids move at velocity $\boldsymbol{v}$ [m/s] in response to spatial differences in fluid pressure P [Pa] in direct proportion to rock permeability κ [m^2] and inverse proportion to fluid viscosity μ [Pa·s],

$$\boldsymbol{v} = \kappa/\mu\ \boldsymbol{\nabla} P. \tag{9}$$

The rate at which fluid diffuses from the stimulation fracture is in part decided by the energetics of the conservation of mass. For an incompressible fluid in a compressible porous medium of elastic bulk modulus B [Pa] the time-evolution of fluid pressure $\partial_t P$ [Pa/s] in a small volume in space is determined by the net flux in and out of the volume given by the divergence of the fluid velocity $\boldsymbol{\nabla}\cdot\boldsymbol{v}$ [1/s] at each point in the fracture system:

$$1/B\ \partial_t P = \boldsymbol{\nabla}\cdot\boldsymbol{v}. \tag{10}$$

Joining gradient flow to pressurisation energetics gives a diffusion equation

$$\partial_t P = \boldsymbol{\nabla}\cdot(B\kappa/\mu)\boldsymbol{\nabla} P = D_f \nabla^2 P, \tag{11}$$

where the second equality assumes material property uniformity gathered into a constant for fluid diffusivity of the medium, $D_f = B\kappa/\mu$ [m^2/s]. As with the heat flow case (3)-(4), the radially symmetric wellbore-centric differential operator expands to $\nabla^2 \equiv \partial_r^{\ 2} + 1/r\ \partial_r$. As in §3, the pressure field solution to (11) in time t and space r associated with fluid flow in the stimulation fracture is then

$$P_0(r,t) = F/(4\pi D t)\ exp(-r^2/4D_f t), \tag{12}$$

with radius r measured from the central wellbore, D_f the effective fluid diffusivity of the stimulation fracture, and F the instantaneous force on a wellbore of effective radius a, [F] = Pa/m^2 = Nt. Expressing diffusivity as $D_f = a^2/4\tau_0$ in terms of the effective wellbore radius a, characteristic fluid drainage flow time τ_0 constant and $P_A \equiv F/A$ for effective wellbore area $A \equiv \pi a^2$, gives

$$P_0(r,t) = P_A\ \tau_0/t\ exp(-r^2/a^2\ \tau_0/t). \tag{12a}$$

From (9), the wellbore-centric radial flow equivalent of (12) follows from the fluid flow velocity $v_0(r,t)$ at radius r and time t as $Q_0(r,t) = 2\pi r v_0(r,t) = 2\pi r\kappa/\mu \partial_r P_0(r,t) = 2\pi r\kappa/\mu P_0(r,t)(-2r/4Dt) = (\pi r^2/Bt)\cdot P_0(r,t)$,

$$Q_0(r,t) = P_A/B\ \pi r^2\ \tau_0/t^2\ exp(-r^2/a^2\ \tau_0/t), \tag{13}$$

[Q_0] = m^2/s. Unlike thermal flow in a porous medium treated above, in our approximation the porosity φ of the stimulated fracture in $Q_0(r,t) = 2\pi r v_0(r,t)$ is assumed to be $\varphi \equiv 1$.

In the absence of other fluid processes associated with fracture stimulation, wellbore production curve data are modelled as occurring at the effective wellbore radius $r = a$ according to a characteristic time τ_0,

$$P_0(a,t) = P_A\ \tau_0/t\ exp(-\tau_0/t), \tag{12b}$$

$$Q_0(a,t) = AP_A/B\ \tau_0/t^2\ exp(-\tau_0/t). \tag{13a}$$

The characteristic model time τ_0 corresponds to the wellbore production curve pressure and flow maxima, $\tau_0 = t_{Pmax}$ and $\tau_0 = 2t_{Qmax}$.

To account for formation fluid draining into the plane of the stimulation fracture, the frack fluid pressure P can be different from ambient formation fluid pressure P_{amb}. Ambient formation fluids flow into the frack in response to the pressure difference given by

$$\partial_t P - D\nabla^2 P = 1/\tau\cdot(P - P_{amb}). \tag{14}$$

The solution to (14) is expressed in terms of the radial solution (12b) by integral form (15) from §1.14 of Carslaw & Jaeger (1959),

$$P(r,t) = P_0\cdot exp(-t/\tau) + 1/\tau_\infty \int_0^t dt' P_0\cdot exp(-t'/\tau_\infty). \tag{15}$$

The additional time constant τ_∞ of (15) gives the time scale on which formation fluid drainage into the frack affects wellbore production fluid flow. For sufficiently large values of τ_∞, $P \approx P_0$ as formation fluids cease to affect wellbore production.

The radial derivative of (13) produces its equivalent expression for flow expressed in terms of flow (13a) associated with pressure $P_0(r,t)$,

$$Q(r,t) = Q_0 \cdot exp(-t/\tau) + 1/\tau \int_0^t dt' Q_0 \cdot exp(-t'/\tau). \quad (16)$$

Denoting the long-term formation-specific time scale as τ_∞, model wellbore production pressure and flow are

$$P(a,t) = P_A \cdot \tau_0 \{1/t \cdot exp(-\tau_0/t - t/\tau_\infty) + 1/\tau_\infty \int_0^t dt'/t' exp(-\tau_0/t' - t'/\tau_\infty)\}, \quad (17)$$

$$Q(a,t) = AP_A/B \cdot \tau_0 \{1/t^2 \cdot exp(-\tau_0/t - t/\tau_\infty) + 1/\tau_\infty \int_0^t dt'/t'^2 exp(-\tau_0/t' - t'/\tau_\infty)\}. \quad (18)$$

As given in Appendix 3, the integral forms (17)-(18) can be simplified for fracture drainage modelling application.

Fig 4 shows sample shale oil production flow histories from fracture-stimulated wellbores. Production curves in blue are overlain by two model curves, green derived from (13) for flow from the fracture only, and red derived from (16) allowing fluid inflow from the formation. The early flow stages for both curves are largely fixed by the peak amplitudes which occur at the characteristic time $\tau_0/2$, τ_0 ~ 20 days. Later-stage flow determines the long-term characteristic time τ_∞, creating a divergence between green and red curves. As summarized in Fig 5, late stage flow is markedly different for oil and gas, τ_∞ ~ 100 days, versus water, τ_∞ ~ 370 days. Water flow is essentially due to frack-flow alone, indicating that the water is a hydrofracture byproduct. This interpretation is supported by Fig 6 well core fluid contents. Since water is reduced at times $t > \tau_\infty$ ~ 100, shale formation outflow is chiefly oil and gas.

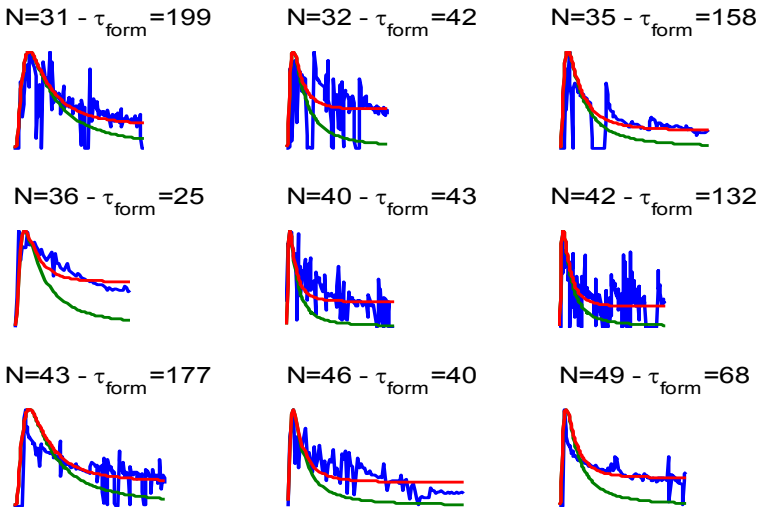

Figure 4: Time-evolving oil flow (blue) from 1.5km-long multi-frack horizontal wellbores in a clastic-like shale formation. Two fits are made to the flow data: green traces for one-parameter model (13) having provision for fracture fluid only, and red traces for two-parameter model (16) having provision for both fracture fluid and formation fluid. Formation fluid flow is required to match observations for oil (shown) and gas (not shown). Formation flow is not required for water (not shown). Above each plot are well number N and formation flow constant in days (τ_∞ in text). The fracture fluid drainage flow constant is τ_0 ~ 20 days.

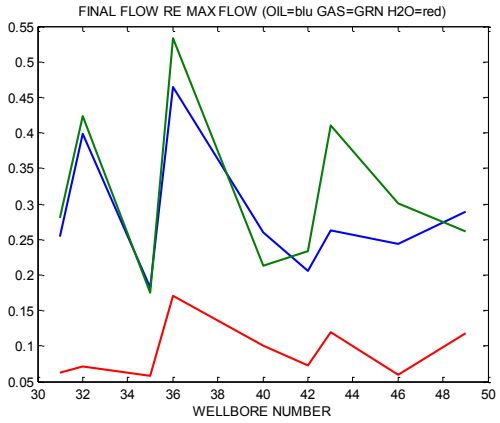

Figure 5: Late state flow relative to maximum flow for nine wellbores; blue = oil, green = gas, red = water. Mean final state oil and gas flows are more than 3 times the mean final state water flow. See Fig 6 for compatible well-core data.

The Fig 5 plot of late-stage flow normalized to peak flow for oil/gas (blue/green) versus water (red) indicates a systematic divergence of shale formation flow of water from shale formation flow of oil/gas. Late stage oil/gas flow averages 35% of peak flow for all wellbore flow data, while late stage water flow averages 10% of peak flow for all wellbores. Fig 6 indicates the probable cause for the fall-off of late stage water flow relative to oil/gas flow. Well-core data at measured depths within the shale formation, MD > 9620ft at plot right, show pores containing approximately 80-90% oil/gas and 10-20% water; the non-shale stratum above the shale formation, MD < 9620ft at plot left, shows equal presence of oil, gas and water.

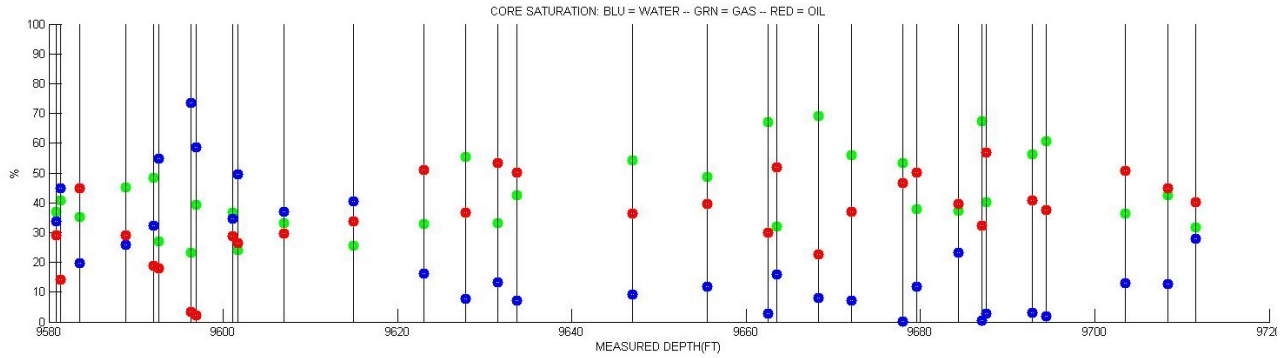

Figure 6: Well core fluid analysis for formation. Horizontal well interval 9620ft to 9720ft has markedly lower water content (blue) than oil (red) and gas (green) in comparison with the stratum above the shale below 9620ft, supporting the interpretation that low wellbore water flow at times greater than τ_∞ is due to its absence in the shale formation.

Late-stage formation flow data can be used to define a frack-formation flow system characteristic time τ_{sys} from which to define the physical scale of the flow system using observed formation production volume and observed formation porosity. While the effective diffusivity D_{sys} of the frack-formation flow system remains unknown, the characteristic system radius $R_{sys} \equiv \sqrt{(D_{sys}/\tau_{sys})}$ must be compatible with reasonably efficient production of the observed fluid volumes according to the model flow and observed characteristic times. Wellbore fluid flow at radii below and above system radius R_{sys}, $r < R_{sys}$ and $r > R_{sys}$, can be expressed in terms of $\alpha = (r/R_{sys})^2$ and wellbore effective area $A = \pi R_{sys}^2$,

$$Q(\alpha,t) = \alpha A P_A/B \cdot \{\tau_0/t^2 \cdot exp(-\alpha\tau_0/t - t/\tau_\infty) + \tau_0/\tau_\infty \int_0^t dt'/t'^2 \cdot exp(-\alpha\tau_0/t' - t'/\tau_\infty)\}. \quad (19)$$

The total volume of produced fluid over succeeding time intervals $[0,T]$ is the integral of (18),

$$V_\alpha(T) = \alpha A P_A/B \cdot \int_0^T dt\ \{\tau_0/t^2 \cdot exp(-\alpha\tau_0/t - t/\tau_\infty) + \tau_0/\tau_\infty \int_0^t dt'/t'^2 \cdot exp(-\alpha\tau_0/t' - t'/\tau_\infty)\}. \quad (20)$$

Fig 7 shows fits of cumulative volumetric flow (20) to oil flow volumes over times $0 < T < 200$ days to provide characteristic times $R_{sys} \equiv \sqrt{(D_{sys}\tau_{sys})}$. The magnitude of flow system radius R_{sys} is estimated from the observed fluid production for an average frack-stimulated formation volume contributing to wellbore flow over the 200 day production interval. Table 1 derives a set of physical parameters for two cases of fluid drainage from the frack-stimulated flow system. The two cases are for, respectively, effectively a maximal 100% and a minimal 10% pore drainage within the flow system. Table 1 summarizes the modelling results for oil, gas, and water.

Table 1: Model fit flow system characteristic radius R_{sys} for cumulative oil, gas, and water production.

FRACK-FORMATION FLUID FLOW SYSTEM	OIL	GAS	WATER
Fluid Volume per Wellbore (bbl)	~ 36000	~ 19400	~ 19200
Fluid Volume per Frack (m^3)	**~ 384**	**~ 207**	**~ 205**
100% Drainage − 5% Porosity Rock Production Volume (m^3)	~ 7680	~ 4140	~ 4100
Characteristic Radius R_{sys} (m)	**~ 23**	**~ 19**	**~ 19**
Diffusivity $D_{sys} = R^2_{sys}/\tau_{sys}$ (m^2/s)	~ 2 10^{-4}	~ 1 10^{-4}	~ 1.5 10^{-4}
Permeability $\kappa_{sys} = \mu B/D_{sys}$ (m^2)	~ 2 10^{-17}	~ 1 10^{-17}	~ 1.5 10^{-17}
10% Drainage − 5% Porosity Rock Production Volume (m^3)	~ 76800	~ 41400	~ 41000
Characteristic Radius R_{sys} (m)	**~ 49**	**~ 40**	**~ 40**
Diffusivity $D_{sys} = R^2_{sys}/\tau_{sys}$ (m^2/s)	~ 8 10^{-4}	~ 4 10^{-4}	~ 6 10^{-4}
Permeability $\kappa_{sys} = \mu B/D_{sys}$ (m^2)	~ 8 10^{-17}	~ 4 10^{-17}	~ 6 10^{-17}

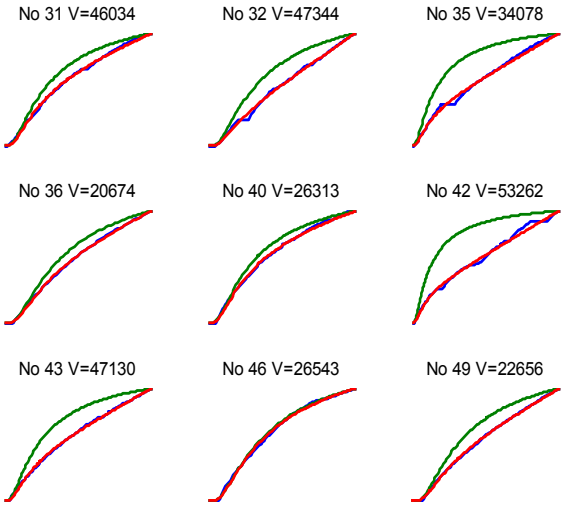

Figure 7: Cumulative oil production curves for nine Fig 4 wellbores. Blue curves show data, green curves show model with frack-specific flow and red curves show model with frack-formation flow. For eight of the nine wellbores, frack-specific flow of radius R does not alone model the cumulative flow data; contributions from the formation are necessary for model agreement. Final production volume in barrels given above plots.

For present purposes the shale-stimulation fluid flow data from nine 1.5km-long production wells summarized in §4 and Table 1 provides essential calibration estimates about hydrofracture stimulation of clastic rock:

- Hydrofracture stimulation of clastic-like shales extends a functional fracture plane radius to perhaps ~ 20 meters as indicated by oil/gas/water trapped in the fracture flowing for ~ 20 days;
- Hydrofracture stimulation of clastic-like shales extends into the formation on either side of the fracture plane, as indicated by oil/gas flowing from the formation into the fracture for ~ 100 days;
- Clastic-like shale formation drainage data implies access to only a small percentage of the potential shale volume;
- The clastic-like nature of hydrocarbon-bearing shales may indicate that hydrofracture stimulation re-activates grain-scale flow channels that were clogged by clays and organic matter rather than creating new flow channels through fresh damage to the clastic-like fabric; if so, the hydrofracture process in clastic-like shales may substantially over-estimate permeability stimulation effects when applied to standard EGS clastic target formations.

5. SUMMARY/CONCLUSIONS

The promise of EGS heat extraction is assessed in terms of irreducible elements: (i) radially-symmetric fluid flow into a long-reach horizontal wellbore from (ii) uniform low-porosity/low-permeability crustal formations subject to wellbore-centric hydro-fracture stimulation and are (iii) embedded in large crustal volumes of capable of conductive and advective heat supply. Assuming the temperature at the wellbore is fixed by the EGS heat extraction process, the properties of such a crustal flow system can be represented by a single parameter, the dimensionless Peclet number $\gamma \equiv v_0 r_0/D$, the ratio of system heat advection to system heat conduction. Wellbore-centric EGS system heat advection is in turn quantified by the Darcy velocity of fluid heat transport flow v_0 at characteristic system radius r_0, with system heat conduction quantified by effective the thermal diffusivity of the rock-fluid combination $D \equiv K/\rho C \sim 4{\cdot}10^{-6}\text{m}^2/\text{s}$ for rock thermal conductivity $K \sim 3\text{W/m}{\cdot}^{\text{o}}\text{C}$ and water volumetric heat capacity $\rho C \sim 1000\text{kg/m}^3{\cdot}4280\text{J/kg}{\cdot}^{\text{o}}\text{C}$. A wellbore-centric heat extraction flow system of Peclet number $\gamma \sim 5$ corresponds to:

- A modest degree of wellbore heat extraction $Q \sim 1$MW per km of wellbore in a crust of porosity $\varphi \sim 10\%$ maintained at fluid exit temperature $T_0 \sim 100^{\text{o}}\text{C}$;
- Effective steady-state heat extraction if the wellbore-centric EGS stimulation volume is 30 to 50 meters in radius;
- The upper limit of practicable wellbore-centric hydraulic fracture stimulation radius given current technical means calibrated by frack-stimulation of low-porosity/low-permeability clastic-like hydrocarbon-bearing shale formations.

Changing the operating environment of this elementary EGS system can somewhat increase the amount of heat extracted and reduce the cost of the system by reducing the amount needed to stimulate the heat exchange flow volume through higher porosity and higher maintained wellbore temperature. However, while in principle the performance of the elementary EGS system can be increased to higher Peclet number, the present analysis suggests considerable caution is needed about achieving a higher Peclet number than, say, 5 as discussed here.

REFERENCES

Bertani R (2015) Geothermal Power Generation in the World 2010-2014 Update Report, *Proceedings World Geothermal Congress,* Melbourne, Australia, 19-25 April 2015.

Bredehoeft JS & Papadopulos IS (1965) Rates of vertical groundwater movement estimated from the Earth's thermal profile, *Water Resources Research* Vol1 No2, 325-328.

Carslaw HS & Jaeger JC (1959) *Conduction of Heat in Solids*, Oxford University Press, pp510.

Jason (2014) Subsurface Characterization Letter Report, JSR-14-Task-013, Miter Corporation, McLean, VA, pp18.

Leary PC (1997) Rock as a critical-point system and the inherent implausibility of reliable earthquake prediction, *Geophysical Journal International* 131, 451-466.

Leary PC (2002) Fractures and physical heterogeneity in crustal rock, in *Heterogeneity of the Crust and Upper Mantle – Nature, Scaling and Seismic Properties*, JA Goff, & K Holliger (eds.), Kluwer Academic/Plenum Publishers, New York, 155-186.

Leary P, Malin P, Geiser P, Pogacnik J, Rugis J & Valles B (2015) Flow Lognormality & Spatial Correlation in Crustal Reservoirs – I: Physical Character & Consequences for Geothermal Energy, *Proceedings World Geothermal Congress 2015*, Melbourne, Australia, 19-25 April 2015.

Malin P, Leary P, Shalev E, Rugis J, Valles B, Boese C, Andrews J & Geiser P (2015) Flow Lognormality and Spatial Correlation in Crustal Reservoirs: II – Where-to-Drill Guidance via Acoustic/Seismic Imaging, *Proceedings World Geothermal Congress 2015*, Melbourne, Australia, 19-25 April 2015.

Moeck IS & Beardsmore G (2014) A new 'geothermal play type' catalog: Streamlining exploration decision making, *Proceedings 39th Workshop on Geothermal Reservoir Engineering*, Stanford University, Stanford, California, February 24-26, 2014.

Pogacnik J, Leary P, Malin P, Geiser P, Rugis J & Valles B (2015) Flow Lognormality and Spatial Correlation in Crustal Reservoirs: III – Natural Permeability Enhancement via Biot Fluid-Rock Coupling At All Scales, *Proceedings World Geothermal Congress 2015*, Melbourne, Australia, 19-25 April 2015.

Tester JW et al. (2006) *The Future of Geothermal Energy -- Impact of Enhanced Geothermal Systems (EGS) on the United States in the 21st Century*, Massachusetts Institute of Technology, pp372.

APPENDIX 1 − In the presence of cylindrically radial flow $v(r) = v_0 r_0/r$, the temperature field (5) written as $T(r) = A + B\,(r/r_0)^{\gamma}$ with $\gamma \equiv v_0 r_0 \rho C/K$, $A \equiv T_0 - (T_1 - T_0)/((r_1/r_0)^{\gamma} - 1)$ and $B \equiv (T_1 - T_0)/((r_1/r_0)^{\gamma} - 1)$ gives heat flow,

$$\begin{aligned} q(r) &= K\partial_r T(r) - \rho C v(r) T(r) \\ &= K\partial_r (A + B\,(r/r_0)^{\gamma}) - \gamma/r\, K(A + B\,(r/r_0)^{\gamma}) \\ &= KB\,(\gamma/r)\,(r/r_0)^{\gamma} - \gamma/r\, KB\,(r/r_0)^{\gamma} - \gamma/r\, KA \\ &= -\gamma/r\, KA \\ &= -\gamma/r\, K\,(T_0 - (T_1 - T_0)/((r_1/r_0)^{\gamma} - 1)). \end{aligned}$$

For situations of interest, $r_1 > r_0$, $\gamma >> 0$, $(T_1 - T_0)/((r_1/r_0)^{\gamma} - 1) \to 0$, hence $q(r) \sim -\gamma/r\, KT_0$.

In the absence of fluid flow, $v(r) = 0$, advective heat flow reduces to thermal conductive heat flow condition $\nabla^2 T(r) = 0$ in the radial domain $r_0 \le r \le r_1$,

$$\begin{aligned} T_{cyl}(r) &= T_0 + (T_1 - T_0)/ln(r_0/r_1)\cdot ln(r_0/r), \\ T_{sph}(r) &= T_0 + (T_1 - T_0)/(r_0/r_1 - 1)\cdot(r_0/r - 1), \\ q_{cyl}(r) &= q_0 r_0/r, \\ q_{sph}(r) &= q_0 r_0^2/r^2, \end{aligned}$$

where q_0 is the flux at the inner radius r_0, $q_0 = K(T_1 - T_0)/r_0/ln(r_0/r_1) < 0$ for cylindrical flow and $q_0 = K(T_1 - T_0)/r_0^2/(1/r_1 - 1/r_0) < 0$ for spherical flow; the negative signs for the heat flow magnitudes indicate inward heat flow.

In the limit of zero Darcy flow velocity, advection forms of heat transport (5)-(6) reduce to the above conduction forms. For (5), expressing exponential function e^x as the limit of $(1 + x/n)^n$ as $n \to \infty$ gives the limiting case $\gamma \to 0$ for the ratio $(x^{\gamma} - 1)/(x_0^{\gamma} - 1)$ as

$$\begin{aligned} (x^{\gamma} - 1)/(x_0^{\gamma} - 1) &= (e^{\gamma ln x} - 1)/(e^{\gamma ln x_0} - 1) \sim ((1 + \gamma ln x/n)^n - 1)/((1 + \gamma ln x_0/n)^n - 1) \\ &\sim (1 + \gamma ln x - 1)/(1 + \gamma ln x_0 - 1) = ln(1/x)/ln(1/x_0). \end{aligned}$$

For (6) in the limit $\gamma \to 0$, $(exp(\gamma(r_0/r - 1)) - 1)/(exp(\gamma(r_0/r_1 - 1)) - 1) \sim (1 + \gamma(r_0/r - 1) - 1)/(1 + \gamma(r_0/r_1 - 1) - 1) = (r_0/r - 1)/(r_0/r_1 - 1)$.

When the inner radius r_0 becomes effectively very large, $r_0 \to \infty$, (3)-(6) revert to the expressions for plane flow geometry for $\gamma/r_0 = v_0/D = v_0\rho C/K$ and $\beta \equiv v_0\rho CL/K$,

$$T_{cyl}(r_0 + \delta r) \propto (1 + \delta r/r_0)^{\gamma} = (1 + \delta r/r_0)^{v0r0/D} \sim exp(v0\delta r/D) = exp(\beta\delta r/L)$$
$$T_{sph}(r_0 + \delta r) \propto exp(\gamma\delta r/r_0) = exp(\delta r v_0\rho C/K) = exp(\beta\delta r/L)$$
$$v_{cyl}(r_0 + \delta r) = v_0/(1 + \delta r/r_0) \sim v_0,$$
$$q_{cyl}(r_0 + \delta r) = Q_0/(1 + \delta r/r_0) \sim Q_0 \equiv v_0\rho C(T_1 - T_0),$$
$$v_{sph}(r_0 + \delta r) = v_0/(1 + 2\delta r/r_0) \sim v_0,$$
$$q_{sph}(r_0 + \delta r) = Q_0/(1 + 2\delta r/r_0) \sim Q_0 \equiv v_0\rho C(T_1 - T_0).$$

APPENDIX 2 − Heat conduction and heat advection time-evolution expressions from Carslaw & Jaeger (1959).

§10.3 I (1) − Instantaneous line-source heat pulse at $r = 0$, $t = 0$ is a purely conductive medium

(1) $T(r,t) = Q/4\pi Dt \cdot exp(r^2/4Dt)$

§15.2 IV (15)-(20) − Instantaneous line-source heat pulse at $r = 0$, $t = 0$

(15) $v(r) \equiv v_0 r_0/r$, radial Darcy fluid flow field
(16) $\partial_r^2 T(r,t) + 1/r\ \partial_r T(r,t) - v(r)/D\ \partial_r T(r,t) - 1/D\ \partial_t T(r,t) = 0$, conservation of heat energy
(17) $\partial_r^2 T(r,s) + 1/r\ (1 - 2\nu)\ \partial_r T(r,s) - k^2 T(r,s) = 0$, $2\nu \equiv v_0 r_0/D$, Laplace transform of (16)
(18) $T(r,s) = r^{\nu} K_{\nu}(kr)$, $K_{\nu}(kr)$ = modified Bessel function of order ν solution to (17)
(19-20) $(kr)^{\nu} K_{\nu}(kr) \to T(r,t) \propto (r^2/4Dt)^{\nu}\ exp(-r^2/4Dt)$, inverse Laplace transform of (18).

§13.5 I (6) − For line-source temperature $T_0 \equiv T(a,0)$, $r > a$ and $t > 0$, pure conduction, $\nu = 0$, in terms of Bessel functions $J_0(kr)$ & $Y_0(kr)$

$$T(r,t) = T_0 + 2/\pi \cdot T_0 \int dk/k\ exp(-k^2Dt)\ (J_0(kr)Y_0(ka) - Y_0(kr)J_0(ka))/(J_0^2(ka) + Y_0^2(ka)^2)$$

§15.2 IV (21) − For line-source temperature $T_0 \equiv T(a,0)$, $r > a$ and $t > 0$, conduction with advection, $\nu > 0$, in terms of Bessel functions $J_{\nu}(kr)$ & $Y_{\nu}(kr)$

$$T(r,t) = T_0 + 2/\pi \cdot T_0\ (r/a)^{\nu} \int dk/k\ exp(-k^2Dt)\ (J_{\nu}(kr)Y_{\nu}(ka) - Y_{\nu}(kr)J_{\nu}(ka))/(J_{\nu}^2(ka) + Y_{\nu}^2(ka)^2)$$

§13.5 I (6) − For heat flux $Q_0 \equiv Q(a,0)$, $r > a$ and $t > 0$, pure conduction, $\nu = 0$,

$$T(r,t) = 2/\pi \cdot Q_0/K \int dk/k^2\ (1\text{-}exp(-k^2Dt))\ (J_0(kr)Y_1(ka) - Y_0(kr)J_1(ka))/(J_1^2(ka) + Y_1^2(ka)^2)$$

Generalize heat flux $Q_0 \equiv Q(a,0)$, $r > a$ and $t > 0$, to conduction with advection, $\nu > 0$,

$$T(r,t) = 2/\pi \cdot Q_0/K \cdot (r/a)^{\nu} \int dk/k^2 (1\text{-}exp(-k^2Dt))(J_{\nu}(kr)Y_{\nu+1}(ka) - Y_{\nu}(kr)J_{\nu+1}(ka))/(J_{\nu+1}^2(ka) + Y_{\nu+1}^2(ka)^2).$$

APPENDIX 3 − The definite form of the integrals in (17-18) have an analytic expression,

$$\int_0^{\infty} dt/t^{1-\nu}\ exp(-\tau_0/t - t/\tau_{\infty}) = 2(\tau_0\tau_{\infty})^{\nu/2}\ K_{\nu}(2\sqrt{\tau_0/\tau_{\infty}}), \quad \text{(A3.1)}$$

where K_{ν} is the modified Bessel function of the second kind; $\nu = 0$ fixes the late-stage pressure term and $\nu = -1$ fixes the late-stage flow term. Analytic expression (17) is useful since for characteristic times that emerge from fitting (15) and (16) to field wellbore flow data, $\tau_0 \sim 20$ days and $\tau_{\infty} \sim 100$ days, the definite integral applies with reasonable accuracy at observation times of order of and greater than characteristic times $t > \tau_{\infty}$,

$$\int_0^{\tau\infty} dt/t^{1-\nu}\ exp(-\tau_0/t - t/\tau_{\infty}) \sim 2(\tau_0\tau_{\infty})^{\nu/2}\ K_{\nu}(2\sqrt{\tau_0/\tau_{\infty}}). \quad \text{(A3.2)}$$

For $\tau_0 \sim 20$ and $\tau_{\infty} \sim 100$, the pressure and flow at τ_{∞} are respectively ~80% and ~96% of their asymptotic values (17). We use (A2) to approximate model flow at times $t > \tau_{\infty} \sim 100$ days at effective radius $r = a$ as in (16) and at larger radii $r > a$ in the extended form of (A3) in which τ_0 is replaced by $\alpha\tau_0$, $\alpha \equiv (r/a)^2$,

$$\int_0^{\tau\infty} dt/t^{1-\nu}\ exp(-\alpha\tau_0/t - t/\tau_{\infty}) \sim 2(\alpha\tau_0\tau_{\infty})^{\nu/2}\ K_{\nu}(2\sqrt{\alpha\tau_0/\tau_{\infty}}). \quad \text{(A3.3)}$$